

PARAMETRIC ANALYSIS OF WING PLANFORMS TO DETERMINE AN OPTIMAL WING DESIGN

Manish Kumar CHAUHAN , Mayur ZOPE  , Srinivasa Rao GORREPATI 

Amity Institute of Defence Technology, Amity University, Noida, Uttar Pradesh, India

Article History:

- received 29 April 2024
- accepted 13 July 2024

Abstract. In designing of Unmanned Aerial Vehicle (UAV), selection of an optimal wing design is a crucial part of complete UAV design process. This research explores the different aerodynamic parameters and the comparison of different wing planforms to ascertain the optimal wing design and improve the overall efficiency of an UAV. The computational analysis using XFLR5 and Open-VSP software is studied to investigate the various aerodynamic parameters of wing. The impact of aspect ratio, taper ratio, wing reference area, coefficient of lift and drag, and stall angle of attack are examined using the Analytical Hierarchy Process (AHP). The results emphasize the importance of different wing planforms and create easier selection of planform for the UAV designers. The study does not only provide the values for operating parameters but also offers practical guidance for design optimization. The semi tapered, and moderate tapered ($\lambda = 0.5$) wings are the good choice to select at the initial phase of design. The highly tapered and elliptical wings provide higher lift but are not efficient in the stalling conditions. Furthermore, the rectangular wing provides elliptical lift distribution, but it is inefficient in the lift generation.

Keywords: wing planform, UAV, lift, drag, stall characteristics, analytical hierarchy process.

 Corresponding author. E-mail: mayurzope1777@gmail.com

1. Introduction

UAVs are continuously evolving for an operations like surveillance and reconnaissance, combat and strike, payload delivery. UAV's efficiency becomes a crucial factor in designing of wing planform. It can be determined by the range, speed, and endurance. These all parameters are depending upon how effectively wing planform generates lift with minimum drag and with safe operation. The selection of an optimal wing planform directly affects aerodynamic efficiency because it directly affects the lift. The overall performance of an UAV can be improved by carefully selecting the wing planform, leading to improved fuel economy, greater endurance, extended range, increased payload carrying capacity and enhanced stability.

Chen and Katz (2004) have investigated the subsonic aerodynamics of aircraft wing, to highlight the effect of aspect ratio, taper ratio, twist, sweep of the wing over induced drag. They have calculated a simple set of data of induced drag values for high aspect ratio wings considering all above parameters. The lifting line theory has been used to analyse the induced drag focussing on a rectangular wing planform and the Fourier series expansion has been used for comparison of elliptical wing lift distribution with the non-elliptical case. They observed that the smaller

taper ratios are essential from structural point of view and higher aspect ratios are desired for lower induced drag. Haque et al. (2015) have compared curved leading edge and rectangular wing planform using NACA 4412 airfoil to determine the effect of wing planform over the various aerodynamic parameters. The experiments have been conducted on both wing planforms at different angle of attack in the wind tunnel. Guzelbey et al. (2018) have been investigated the effect of taper ratio over wing induced drag coefficient, lift coefficient, and spanwise lift distribution and also discussed the optimization of these parameters to achieve the required aircraft efficiency. XFLR5 tool is used for analysis of wings and to get the experimental values for comparison. An optimum taper ratio has been observed to reduce the induced drag coefficient and improved the efficiency of wingspan. The authors also examined the formation of tip vortices for each wing design to minimize the tip vortex. Dhekane and Sherje (2020) have conducted an analysis of wing of S1223 airfoil based on lift coefficient, and structural strength with different taper ratio. As the taper ratio increases, the lift distribution curve became close to rectangular shape showing maximum local lift coefficient near to wingtip. They developed a methodology to divide the wing into equal parts and showed that the moderate taper ratio of 0.4 or 0.5 could

perform well and provide lift distribution close to elliptical distribution.

Daniel (2020) investigated the performance of asymmetric airfoil using XFLR5 software and explained the way to select an airfoil of UAV for optimum performance. Hamurcu and Eren (2020) explained the integration of multicriteria decision making technique to select the optimum UAV among available options. AHP technique is used to determine category weights and TOPSIS is used to rate alternatives for selecting best UAV. Hospodář et al. (2022) observed the effects of different wing planforms over lift distribution to minimize the drag coefficient, to reduce structural weight and flight performance assessment for fuel economy. The results showed an aircraft with bell-shaped lift distribution can provide 4–6% better fuel efficiency compared with the elliptical wing planform. The selection of an optimal wing planform plays an important role in UAV designing. Saraçyakupoğlu et al. (2022) focused on design of loitering munition UAV system capable of day and night operation, with flight time of 2 to 3 hrs. and to be catapult launched. They analyzed different methodologies used in UAV construction and setting a strong foundation for UAV design. They also performed the experimental and numerical analysis to study various parameters of UAV and demonstrated that the loiter munition UAV system is reliable and cost efficient for operations in defense and security missions. Akdeniz (2020) investigated the effect of a flap design over aerodynamic and flight characteristics of the NACA 4415 airfoil using XFLR 5 software. A comparison is made between the original NACA 4415 wing design and modified $+5^\circ$ flapped design considering Reynolds number and angle of attack, showed significant increase in lift force. Alam et al. (2014) fabricated an UAV with airfoil shaped fuselage using NACA 4416 airfoil and compared different aerodynamic characteristics using CFD analysis. They studied the design parameters of airfoil shaped fuselage UAV model using open circuit subsonic wind tunnel considering range of Reynolds number at varying angle of attack.

Palic and Lalic (2009) discussed important tool for decision making in various scenario using AHP technique. They showed major strength of AHP and outlined its systematic approach to minimize subjective decision making when choosing between different alternatives. Khan and Faruk (2018) compared the aerodynamic performance of NACA 2412 airfoil wing with and without curved leading edge. Two wing models were analyzed using CFD simulations, where curved leading edge wing planform demonstrated higher lift and comparatively lower drag leading to higher lift to drag ratio. Siddiqi and Lee (2019) focused on modifying the wing of an UAV RQ-7 Shadow to investigate the changes in aerodynamic characteristics, including modifications in airfoil, wing planform, aspect ratio and adding winglets. CFD analysis for five different wing planforms have been carried out using ANSYS Fluent software to calculate the lift to drag ratio at various angle of attacks and speeds.

Karpenko et al. (2023) performed theoretical and experimental research on aerospace laminated composite structure using frequency analysis. Various samples were made using extruded polystyrene and the vibrational damping characteristics of the material tested using piezoelectric micro vibration test. Das and Roy (2018) aims to compare different composite materials to replace Aluminium 2024 T3 because of their high strength to weight ratio and fatigue life. The study focused on structural analysis of wing structure to evaluate wing performance using CATIA V5 R20 and ANSYS software. Jadhav (2020) compared structural behaviour of Boeing BACXXX airfoil wing under loading conditions made from aluminium alloy and titanium alloy. CATIA V5 R21 and ANSYS software are used for wing structure design and analysis of wing respectively. Kirubakaran et al. (2017) investigated optimization of aircraft wing weight using composite material design, comparing metallic and composite structure to analyze structural properties and stress distribution using CATIA V5 and ANSYS softwares. Lubecki et al. (2022) studied the use of composite materials for reduction of weight and energy consumption of mechanical components. They developed hydraulic cylinder design using composite material to reduce the weight and focussed on the effect of weight reduction over bending moment cused in the boom of working machines.

Nowadays, various types of wing planforms are available, but there are no established criteria for the optimal selection of a wing based on different parameters while considering the effect of varying camber and airfoil thickness. The present study is mainly focused on determining the optimal wing planform by comparing them using AHP technique, based on the effects of varying camber, airfoil thickness, coefficient of lift, drag, and stall characteristics. Figure 1 shows the basic wing terminology which is used to design a wing in preliminary stage of an aircraft design. Root chord (C_r) is the length of the wing section near to the fuselage. Tip chord (C_t) is the length of wing section at the end of the wing. Span (b) represents the total wing length from one side to other. Wing area (S) represents total wing reference area of an aircraft wing (Sadraey, 2013).

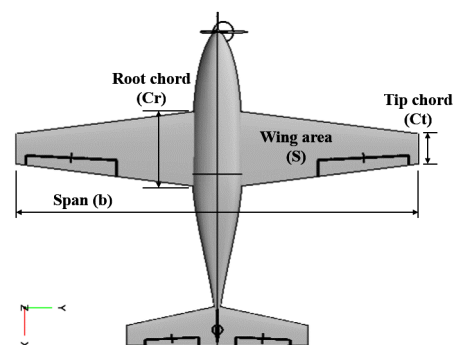


Figure 1. Terminology of wing

1.1. Aerodynamic parameters

The aerodynamic parameters are associated with wing geometry and used to determine the aerodynamic performance of the wing. These parameters play an important role to design wing in initial phase.

1.1.1. Lift coefficient

The coefficient of lift is a dimensionless parameter which is used to evaluate lift force generated by an airfoil and wing. Equations (1)–(4) represent the theoretical way to calculate lift coefficient for an airfoil as well as for a finite wing based on lift slope value which are dimensionless parameters (Sadraey, 2013; Gudmundsson, 2022).

$$\text{Airfoil Lift slope, } C_{l\alpha} = 1.8 \times \pi \left(1 + 0.8 \times \frac{t_{\max}}{c} \right). \quad (1)$$

$$\text{Airfoil coefficient of lift, } C_l = C_{l\alpha} \times (\alpha - \alpha_{L=0}). \quad (2)$$

$$\text{Wing lift slope, } C_{L\alpha} = \frac{C_{l\alpha}}{1 + (57.3 \times K \times C_{l\alpha})}. \quad (3)$$

$$\text{Wing coefficient of lift, } C_L = C_{L\alpha} \times (\alpha - \alpha_{L=0}). \quad (4)$$

1.1.2. Drag coefficient

Drag coefficient is the dimensionless quantity which characterizes total drag force experienced by an aircraft while it moves through an air. Total drag coefficient is a combined effect of lift induced drag and parasitic drag. Equation (5) represents drag polar which provides the value for total drag coefficient of an aircraft (Guzelbey et al., 2018).

$$\text{Total drag coefficient, } C_D = C_{D0} + K (C_L^2). \quad (5)$$

The lift induced drag is generated due to the lift generation of the wing. When an aircraft lifts, it creates vortices at the wing tip and due to this a backward force vector adds on total drag. It is directly proportional to lift generated and inversely proportional to aspect ratio of the wing. High aspect ratio wing produces less lift induced drag compared with low aspect ratio wing. Parasitic drag is caused by the shape, surface, and all other non-lift producing components. It is a result of form drag which cause by the shape of moving body through fluid, skin friction dracause due to the friction between the body surface and fluid, and interference drag cause when an airflow gets disturb with an aircraft component and this disturbed air



Figure 2. High angle of attack

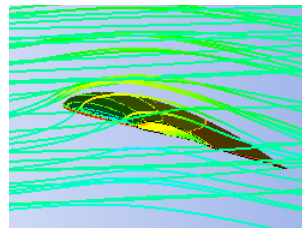


Figure 3. Low angle of attack

flows over other components (Sadraey, 2013; Gudmundsson, 2022).

1.2. Stall characteristics

Stalling is a main constraint in preliminary design of an aircraft. In fixed wing UAV, aircraft must exceed stalling speed for safe take-off. It is the minimum speed which is required for an aircraft to fly.

1.2.1. Stall angle

Gudmundsson (2022) and Hospodář et al. (2022) explained that stall is a condition in aircrafts. If the angle of attack increases, the lift starts decreasing which is known as critical angle of attack. If the angle of attack increases beyond this limit, there would be sudden drop in lift generated by the wing and aircraft becomes unstable leading to the higher risk of losing control.

Figures 2–3 represents the flow over a wing at high and low angle of attack. These figures are general representation of flow over the wing to highlight a difference between flow lines over the wing at lower and higher angle of attack. Flow remains attached for low angle of attack and generates the required lift. As the angle of attack increases, the flow is separated near to top leading edge and lift of wing is reduced. Hence it is important to know the stall angle of attack before designing an actual wing. Stall angle can be easily predicted by using following parameters. First the maximum lift coefficient of wing is required without sweep, twist, or any dihedral angle. Equation (6) represents maximum lift coefficient of wing with no sweep. After that aspect ratio of wing should be matched the criteria. Equation (7) represents the aspect ratio criteria for high aspect ratio wing. After that leading edge parameter is calculated by Δy . For NACA 4 or 5 series, the value for Δy is given by 25 (t/c). Finally, stall angle of attack for finite wing is calculated by the theoretical formula represented in Equation (8).

$$C_{L\max} = 0.9 \times C_{L\max i} \quad (6)$$

$$AR > \frac{4}{(C_1 + 1) \cos \Lambda_{LE}}; \quad (7)$$

$$\alpha_{Stall} = \frac{C_{L\max}}{C_{L\alpha}} + \alpha_{ZL} + \Delta \alpha_{Stall}. \quad (8)$$

2. Methodology

2.1. Prerequisites

For parametric analysis of the fixed wing UAV, the value of basic parameters is considered which are mentioned in Table 1. Normally, wing span should be 3–9 m for small and medium type of UAV, and the speed ranges should be from 6–18 m/s. In this study, 6 m wing span with 1 m root chord and 10 m/s are selected to ease the calculations (Dhekane & Sherje, 2020).

Table 1. Value of considered parameters

| Parameter | Value |
|------------------------------------|------------------------------|
| Span (b) | 6 m |
| Root chord (C_r) | 1 m |
| Speed (V) | 10 m/s |
| Density (ρ) | kg/m ³ |
| Oswald's span efficiency (e) | 0.8 |
| Dynamic viscosity of air (μ) | 0.00001789 Ns/m ² |

2.2. Modelling

Fixed wing UAVs rely on a variety of airfoils or wing profiles to achieve the desired aerodynamic performance. The selection of an airfoil is crucial to determining an UAV's flight characteristics, efficiency, and mission capabilities. Small and medium type of UAV uses various type of materials for wing structure, each material offers unique properties to maintain structural stability. The choice of material depends upon various factors like strength to weight ratio, cost, flexibility, thermal properties (Das & Roy, 2018; Jadhav, 2020). Metals like aluminium and titanium are comparatively lighter in weight than steel, but are heavier than composite materials. Composite materials provide better corrosion resistance, excellent strength to weight ratio and good impact resistance (Karpenko et al., 2023; Kirubakaran et al., 2017).

NACA airfoils are available in open source and easily manufacturable. Two cases are considered based on change in camber and thickness of NACA airfoil which are commonly used for fixed wing design (Akdeniz, 2020).

Case I – Increasing camber – NACA 1412, NACA 2412, NACA 4412, NACA 6412.

Case II – Increasing thickness – NACA 4412, NACA 4418, NACA 4421, NACA 4424.

Several wing planforms are available to design the UAVs, but certain designs are more commonly employed due to their suitability for different mission profiles. Five wing planforms are selected for the study as Elliptical wing, Rectangular wing ($\lambda = 1$), Moderate tapered wing ($\lambda = 0.5$), Highly tapered wing ($\lambda = 0.3$), and Semi tapered wing ($\lambda = 0.5$ for tapered section) which are shown in Figure 4. The average value for taper ratio is 0.5, which is selected for moderate tapered wing. Semi-tapered wing is the combination of rectangular and tapered wing and by maintaining the same taper ratio as moderate tapered wing, this wing planform show combined characteristics of rectangular and moderate tapered wing, which help this study in better position to identify how the planform geometry affects key aerodynamic parameters. The lower value of taper ratio increases the local lift coefficient value near to wing tip which increase the chances of stalling of an aircraft at much lower angle of attack (Siddiqi & Lee, 2019; Khan & Faruk, 2018).

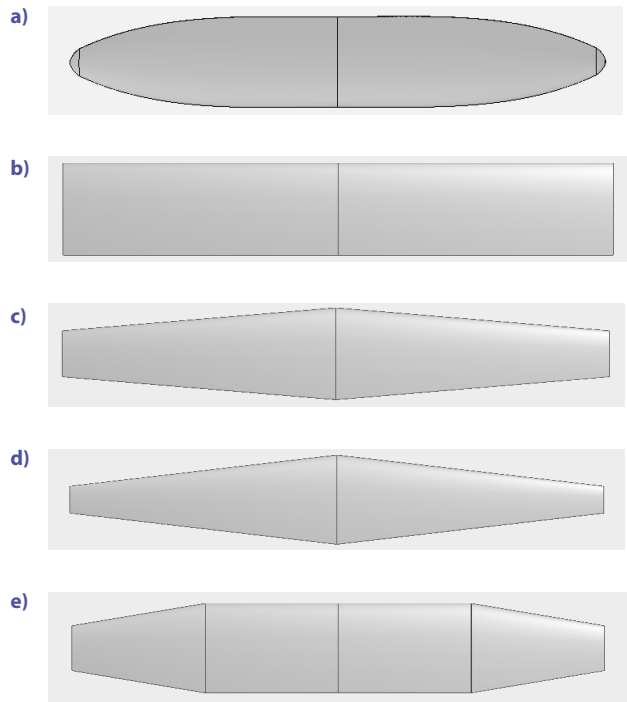


Figure 4. Geometry of different wing planforms for small and medium category UAVs: a – elliptical wing; b – rectangular wing; c – moderate tapered wing; d – highly tapered wing; e – semi tapered wing

2.3. Wing analysis

Analysis is carried out with the help of XFLR5 solver and Open VSP solver using 3 D panel method. Reynolds number has significance in analysis as the lift generated is highly dependent on it. Reynolds number (R_e) is calculated by Equation (9).

$$R_e = \frac{\rho V D}{\mu} \quad (9)$$

In this research, the range of characteristic length (D) from minimum chord length of 0.3 m to maximum chord length of 1 m is considered and based on this, the Reynolds number is calculated and the range is selected from 2×10^5 to 7×10^5 for characteristics length of 0.3 m to 1 m (Alam et al., 2014; Saraçyakupoğlu et al., 2022).

2.3.1. Lift and drag

Computational analysis is performed for all wing planforms and the values for lift coefficient, induced and parasitic drag coefficient, total drag coefficient is obtained for case I and Case II of airfoils in Table 2 and Table 3 respectively. Wing analysis data with increasing airfoil camber and thickness is used for parametric comparison using AHP technique.

Table 2. Wing analysis data with increasing airfoil camber

| | Wing type | Aspect ratio | Tapered ratio (λ) | Angle of attack (α) deg. | Coefficient of lift (C_L) | Induced drag (C_{Di}) | Parasitic drag (C_{Do}) | Total drag (C_D) |
|-----------|------------------|--------------|-----------------------------|-----------------------------------|-------------------------------|---------------------------|-----------------------------|----------------------|
| NACA 1412 | Rectangular | 6 | 1 | 2 | 0.232 | 0.00285 | 0.00613 | 0.00898 |
| | moderate tapered | 8 | 0.5 | 2 | 0.263 | 0.00271 | 0.00685 | 0.00956 |
| | highly tapered | 9.23 | 0.3 | 2 | 0.268 | 0.00243 | 0.00722 | 0.00965 |
| | semi tapered | 6.86 | 0.5 | 2 | 0.248 | 0.0028 | 0.00642 | 0.00922 |
| | Elliptical wing | 8.99 | – | 2 | 0.290 | 0.00315 | 0.0123 | 0.0155 |
| NACA 2412 | Rectangular | 6 | 1 | 2 | 0.311 | 0.00513 | 0.00619 | 0.01133 |
| | moderate tapered | 8 | 0.5 | 2 | 0.353 | 0.00488 | 0.00686 | 0.01173 |
| | highly tapered | 9.23 | 0.3 | 2 | 0.358 | 0.00434 | 0.0072 | 0.01154 |
| | semi tapered | 6.86 | 0.5 | 2 | 0.333 | 0.00501 | 0.00643 | 0.01144 |
| | Elliptical wing | 8.99 | – | 2 | 0.388 | 0.00566 | 0.0126 | 0.0183 |
| NACA 4412 | Rectangular | 6 | 1 | 2 | 0.467 | 0.01163 | 0.00725 | 0.01888 |
| | moderate tapered | 8 | 0.5 | 2 | 0.533 | 0.01045 | 0.00741 | 0.01789 |
| | highly tapered | 9.23 | 0.3 | 2 | 0.536 | 0.00974 | 0.00772 | 0.01746 |
| | semi tapered | 6.86 | 0.5 | 2 | 0.499 | 0.01129 | 0.00723 | 0.01852 |
| | Elliptical wing | 8.99 | – | 2 | 0.582 | 0.01275 | 0.01355 | 0.02629 |
| NACA 6412 | Rectangular | 6 | 1 | 2 | 0.622 | 0.02064 | 0.00902 | 0.02965 |
| | moderate tapered | 8 | 0.5 | 2 | 0.710 | 0.0197 | 0.00949 | 0.02919 |
| | highly tapered | 9.23 | 0.3 | 2 | 0.713 | 0.01721 | 0.00985 | 0.02707 |
| | semi tapered | 6.86 | 0.5 | 2 | 0.663 | 0.01998 | 0.00922 | 0.0292 |
| | Elliptical wing | 8.99 | – | 2 | 0.750 | 0.02115 | 0.01466 | 0.0358 |

Table 3. Wing analysis data with increasing airfoil thickness

| | Wing type | Aspect ratio | Tapered ratio (λ) | Angle of attack (α) deg. | Coefficient of lift (C_L) | Induced drag (C_{Di}) | Parasitic drag (C_{Do}) | Total drag (C_D) |
|-----------|------------------|--------------|-----------------------------|-----------------------------------|-------------------------------|---------------------------|-----------------------------|----------------------|
| NACA 4412 | Rectangular | 6 | 1 | 2 | 0.467 | 0.01163 | 0.00724 | 0.01888 |
| | moderate tapered | 8 | 0.5 | 2 | 0.533 | 0.01045 | 0.00744 | 0.0179 |
| | highly tapered | 9.23 | 0.3 | 2 | 0.536 | 0.00974 | 0.00773 | 0.01747 |
| | semi tapered | 6.86 | 0.5 | 2 | 0.499 | 0.01129 | 0.00723 | 0.01853 |
| | Elliptical wing | 8.99 | – | 2 | 0.582 | 0.01275 | 0.01355 | 0.02629 |
| NACA 4418 | Rectangular | 6 | 1 | 2 | 0.481 | 0.01234 | 0.00921 | 0.02155 |
| | moderate tapered | 8 | 0.5 | 2 | 0.534 | 0.01112 | 0.0097 | 0.02081 |
| | highly tapered | 9.23 | 0.3 | 2 | 0.554 | 0.01037 | 0.01009 | 0.02047 |
| | semi tapered | 6.86 | 0.5 | 2 | 0.513 | 0.01196 | 0.00942 | 0.02138 |
| | Elliptical wing | 8.99 | – | 2 | 0.585 | 0.01294 | 0.01355 | 0.02651 |
| NACA 4421 | Rectangular | 6 | 1 | 2 | 0.487 | 0.01264 | 0.01024 | 0.02289 |
| | moderate tapered | 8 | 0.5 | 2 | 0.541 | 0.0114 | 0.01089 | 0.0223 |
| | highly tapered | 9.23 | 0.3 | 2 | 0.561 | 0.01065 | 0.0114 | 0.02205 |
| | semi tapered | 6.86 | 0.5 | 2 | 0.520 | 0.01224 | 0.01054 | 0.02278 |
| | Elliptical wing | 8.99 | – | 2 | 0.588 | 0.01311 | 0.0136 | 0.0267 |
| NACA 4424 | Rectangular | 6 | 1 | 2 | 0.493 | 0.01294 | 0.01131 | 0.02425 |
| | moderate tapered | 8 | 0.5 | 2 | 0.548 | 0.01169 | 0.01217 | 0.02386 |
| | highly tapered | 9.23 | 0.3 | 2 | 0.568 | 0.01092 | 0.01279 | 0.02371 |
| | semi tapered | 6.86 | 0.5 | 2 | 0.526 | 0.01252 | 0.01168 | 0.02419 |
| | Elliptical wing | 8.99 | – | 2 | 0.589 | 0.01315 | 0.0136 | 0.02676 |

2.3.2. Stall angle

Stall angle of attack is calculated using Equation (8). The calculated value of Lift slope, maximum lift coefficient, and

stall angle of attack is shown in Table 4 for the airfoils of case I and case II.

Table 4. Variation of stall angle of attack for different airfoils

| Airfoil | Planform | Cl_α | CL_α | Cl_{max} | CL_{max} | α_{zL} | $\Delta\alpha_{stall}$ | α_{stall} |
|-----------|------------------|-------------|-------------|------------|------------|---------------|------------------------|------------------|
| | | /deg. | /deg. | | | deg. | | deg. |
| NACA 1412 | Rectangular | 0.108 | 0.0766 | 1.3662 | 1.23 | -1.10 | 0 | 14.95 |
| | Moderate tapered | 0.108 | 0.0826 | 1.0362 | 0.93 | -1.10 | 1.212 | 11.40 |
| | highly tapered | 0.108 | 0.0853 | 0.9369 | 0.84 | -1.10 | 1.212 | 10.00 |
| | semi tapered | 0.108 | 0.0795 | 1.0296 | 0.93 | -1.10 | 1.212 | 11.77 |
| | elliptical | 0.108 | 0.0848 | 1.2128 | 1.09 | -1.12 | 1.212 | 12.96 |
| NACA 2412 | Rectangular | 0.108 | 0.0766 | 1.4392 | 1.30 | -2.22 | 0 | 14.69 |
| | Moderate tapered | 0.108 | 0.0826 | 1.0949 | 0.99 | -2.25 | 1.212 | 10.89 |
| | highly tapered | 0.108 | 0.0853 | 0.9999 | 0.90 | -2.26 | 1.212 | 9.50 |
| | semi tapered | 0.108 | 0.0795 | 1.0880 | 0.98 | -2.22 | 1.212 | 11.31 |
| | elliptical | 0.108 | 0.0848 | 1.2705 | 1.14 | -2.24 | 1.212 | 12.45 |
| NACA 4412 | Rectangular | 0.108 | 0.0766 | 1.5555 | 1.40 | -4.30 | 0 | 13.98 |
| | Moderate tapered | 0.108 | 0.0826 | 1.1690 | 1.05 | -4.34 | 1.212 | 9.61 |
| | highly tapered | 0.108 | 0.0853 | 1.0857 | 0.98 | -4.35 | 1.212 | 8.32 |
| | semi tapered | 0.108 | 0.0795 | 1.1612 | 1.05 | -4.30 | 1.212 | 10.06 |
| | elliptical | 0.108 | 0.0848 | 1.3727 | 1.24 | -4.32 | 1.212 | 11.46 |
| NACA 6412 | Rectangular | 0.108 | 0.0766 | 1.6470 | 1.48 | -6.32 | 0 | 13.03 |
| | Moderate tapered | 0.108 | 0.0826 | 1.2839 | 1.16 | -6.59 | 1.212 | 8.61 |
| | highly tapered | 0.108 | 0.0853 | 1.1526 | 1.04 | -6.53 | 1.212 | 6.84 |
| | semi tapered | 0.108 | 0.0795 | 1.2766 | 1.15 | -6.32 | 1.212 | 9.35 |
| | elliptical | 0.108 | 0.0848 | 1.4815 | 1.33 | -6.34 | 1.212 | 10.59 |
| NACA 4412 | Rectangular | 0.108 | 0.0766 | 1.5555 | 1.40 | -4.30 | 0 | 13.98 |
| | Moderate tapered | 0.108 | 0.0826 | 1.1690 | 1.05 | -4.34 | 1.212 | 9.61 |
| | highly tapered | 0.108 | 0.0853 | 1.0857 | 0.98 | -4.35 | 1.212 | 8.32 |
| | semi tapered | 0.108 | 0.0795 | 1.1612 | 1.05 | -4.30 | 1.212 | 10.06 |
| | elliptical | 0.108 | 0.0848 | 1.3727 | 1.24 | -4.32 | 1.212 | 11.46 |
| NACA 4418 | Rectangular | 0.113 | 0.0789 | 1.6058 | 1.45 | -4.27 | 0 | 14.04 |
| | Moderate tapered | 0.113 | 0.0853 | 1.2311 | 1.11 | -4.32 | 2.179 | 10.84 |
| | highly tapered | 0.113 | 0.0882 | 1.0405 | 0.94 | -4.34 | 2.179 | 8.46 |
| | semi tapered | 0.113 | 0.0820 | 1.2236 | 1.10 | -4.27 | 2.179 | 11.33 |
| | elliptical | 0.113 | 0.0877 | 1.4346 | 1.29 | -4.29 | 2.179 | 12.61 |
| NACA 4421 | Rectangular | 0.115 | 0.0801 | 1.6072 | 1.45 | -4.22 | 0 | 13.84 |
| | Moderate tapered | 0.115 | 0.0867 | 1.2372 | 1.11 | -4.30 | 2.179 | 10.72 |
| | highly tapered | 0.115 | 0.0896 | 0.9938 | 0.89 | -4.32 | 2.179 | 7.84 |
| | semi tapered | 0.115 | 0.0833 | 1.2298 | 1.11 | -4.22 | 2.179 | 11.25 |
| | elliptical | 0.115 | 0.0891 | 1.4348 | 1.29 | -4.24 | 2.179 | 12.43 |
| NACA 4424 | Rectangular | 0.118 | 0.0812 | 1.5725 | 1.42 | -4.12 | 0 | 13.30 |
| | Moderate tapered | 0.118 | 0.0880 | 1.2108 | 1.09 | -4.27 | 2.179 | 10.29 |
| | highly tapered | 0.118 | 0.0911 | 0.9766 | 0.88 | -4.30 | 2.179 | 7.53 |
| | semi tapered | 0.118 | 0.0845 | 1.2036 | 1.08 | -4.12 | 2.179 | 10.88 |
| | elliptical | 0.118 | 0.0905 | 1.4076 | 1.27 | -4.17 | 2.179 | 12.00 |

2.3.3. Stall region over wing span

The lift distribution over different type of wing span is represented in Figure 5 by solving wing analysis in XFLR5. As the angle of attack increases beyond the critical angle of attack, stall occurs first at the point of maximum local lift coefficient and propagates from that portion over the wing span. The mounting of an ailerons should be avoided in this region because in case of stall, these control surfac-

es play an important role to control an aircraft (Guzelbey et al., 2018; Hospodář et al., 2022).

For rectangular wing, the maximum local lift coefficient occurs at a root chord and this makes more efficient in stalling conditions. As the taper ratio increases, the maximum local lift coefficient shifts towards wingtip and the stall region closer to an ailerons. If an aircraft enters into the stalling, the lift is suddenly loss near to the tip region making an aircraft uncontrollable (Dhekane & Sherje,

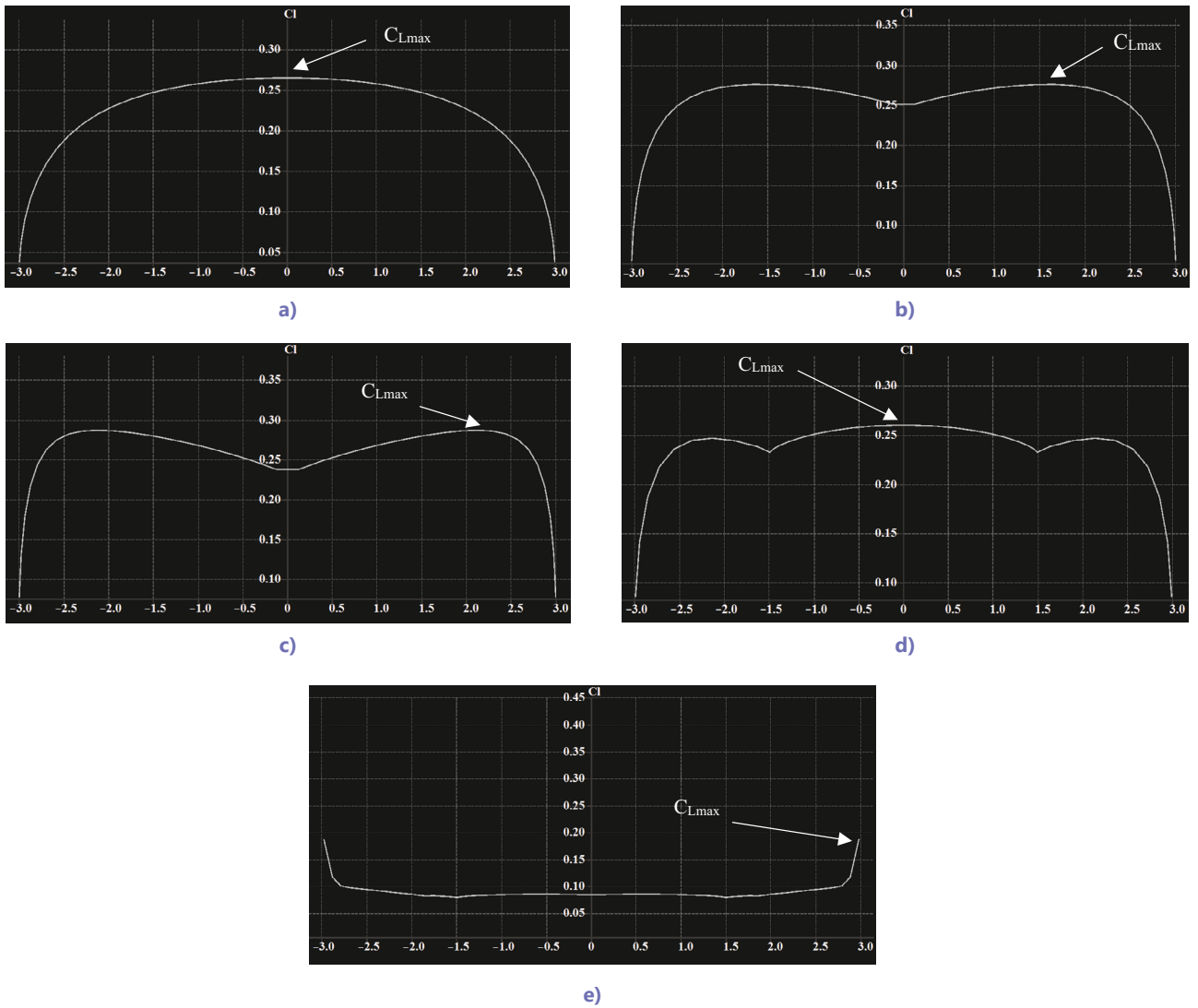


Figure 5. Lift distribution over different type of wing planforms: a – rectangular wing; b – moderate tapered wing ($\lambda = 0.5$); c – highly tapered wing ($\lambda = 0.3$); d – semi tapered wing; e – elliptical wing

2020). In semi tapered wings, the local lift coefficient is maximum at a root chord, similar to the rectangular wing planform, which puts an aileron out of the stalling region and aircraft can be easily controlled. Stall region is easily predictable using this method for any type of wing during the conceptual stage of UAV design (Gudmundsson, 2022).

2.3.4. Effect of camber and thickness of an airfoil

The effect of increasing camber and thickness of airfoils is shown in Figure 6 and 7 respectively. Figures show the variation of lift coefficient with reference to angle of attack (α). The airfoil analysis is done at Mach number of 0.03 and Reynolds number of 6.85×10^5 .

As the camber increases, the flow over an airfoil accelerates which creates more negative pressure on the upper side and thus lift generated by the wing increases, this shifts the lift slope slightly upward. Increasing camber provides the positive value of lift at zero angle of attack but it decreases the stalling angle of attack significantly. Stall

angle is the value of α where the curve achieves the maximum value of lift. Figure 6 represents a sharp drop in the lift after stall angle of attack. Increasing thickness does not show significant effect on stall characteristics of

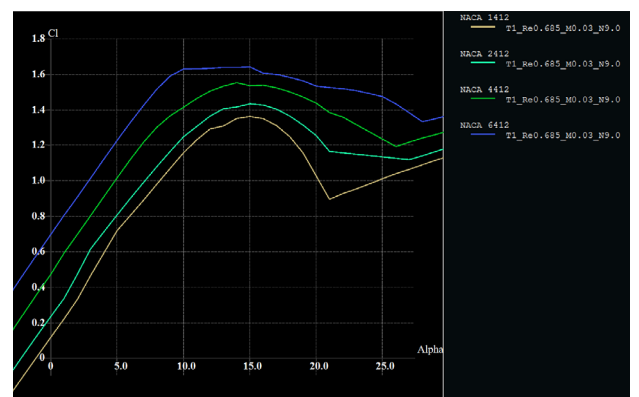


Figure 6. Effect of increasing camber

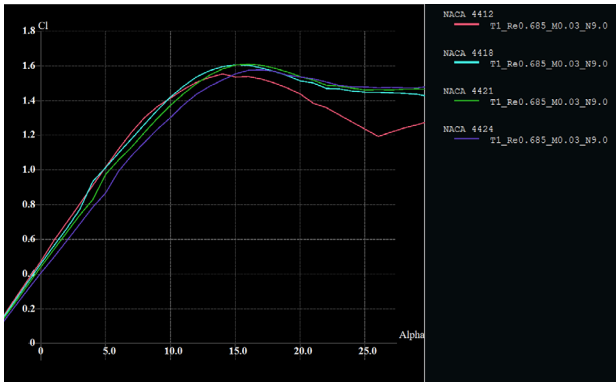


Figure 7. Effect of increasing thickness

a wing. Lift slightly increases for moderate thickness of an airfoil but parasitic drag increases with thickness. It provides smooth stalling behavior as compared with increasing camber airfoils (Daniel, 2020; Gudmundsson, 2022).

3. Results and discussion

AHP is the multi-criteria decision-making technique which is used to compare various available alternatives to identify best possible option. This process uses different criteria and sub criteria to obtain category weights by giving ratings with the help of experts (Bhushan & Rai, 2004). After computational analysis of 3D wing geometries, all the values of wing aerodynamic parameters and stall characteristics are used to compare wing planforms. AHP technique is used to study the parametric analysis of different wing planforms with increase in camber and thickness of airfoil (Hamurcu & Eren, 2020; Palcic & Lalic, 2009).

3.1. Camber of an airfoil

Figures 8–13 represent the analysis of wing planforms with increasing camber of an airfoil using AHP technique. As the camber increases, the lift also increases for all wing planforms. Coefficient of lift is not only depending upon the camber but also upon the taper ratio. High taper ratio increases lift generation, but this shifts the local maximum lift coefficient towards wingtip which causes the tip of the wing to stall. If the tip stalls first, the aircraft becomes unstable, and the lift is suddenly loss closer to wingtip (Haque et al., 2015). The induced drag is inversely proportional to the aspect ratio. When the aspect ratio is high, the induced drag decrease which reduces the total drag of a wing planform; and the length of a wing increases which makes the lift distribution close to elliptical distribution and distributes the lift gradually over the span, minimizing the vortices at the tip (Chen & Katz, 2004). Parasitic drag is highly depending upon the shape and skin friction of a wing. Due to the high aspect ratio, tapered wings show better drag characteristics, but these are inefficient in comparison of stall characteristics. In high tapered wings, the stall region over the span moves towards the wingtip. Ailerons are required to mount outwards near to the tip for better effectiveness

in controlling the roll of an aircraft; putting ailerons in the stall region makes them ineffective during the stalling conditions and increases the risk of losing control of an aircraft. Semi tapered wing shows better stall characteristics than the other wing planforms. Due to rectangular section at the middle, these wings have maximum local lift coefficient at a root chord, making them more efficient in the stalling conditions (Guzelbey et al., 2018).

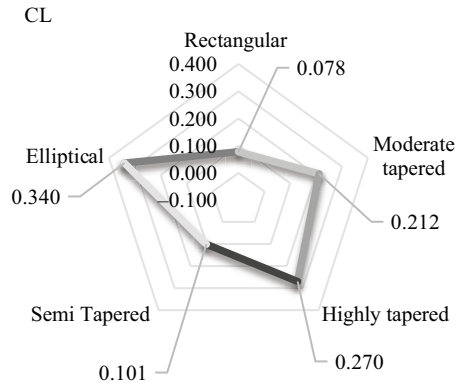


Figure 8. AHP result based on coefficient of lift

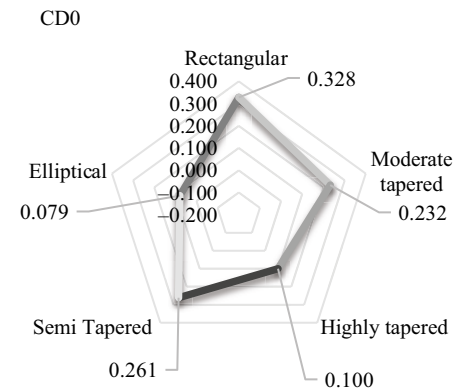


Figure 9. AHP result based on coefficient of parasitic drag

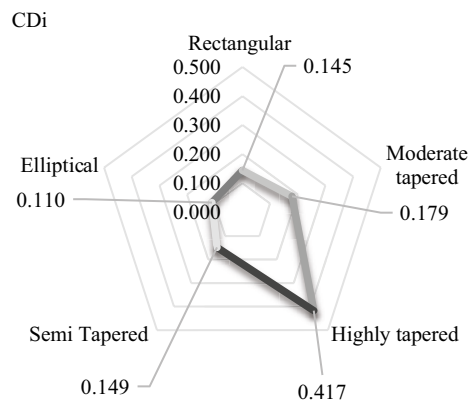


Figure 10. AHP result based on coefficient of induced drag

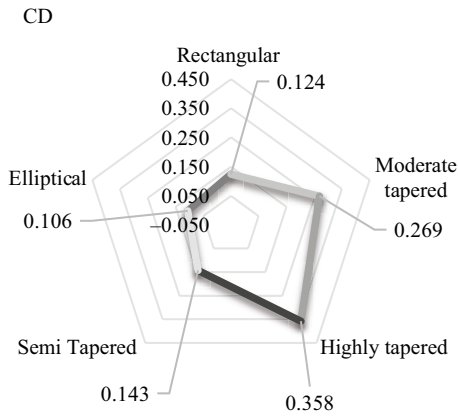


Figure 11. AHP result based on coefficient of total drag

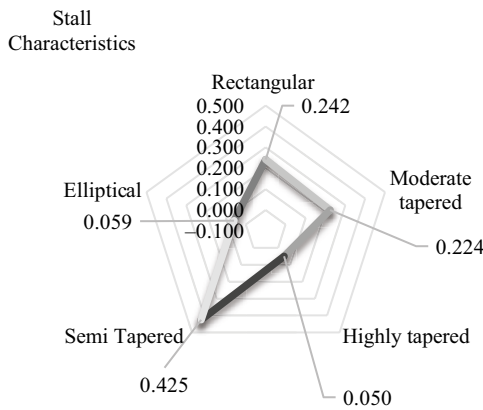


Figure 12. AHP result based on stall characteristics

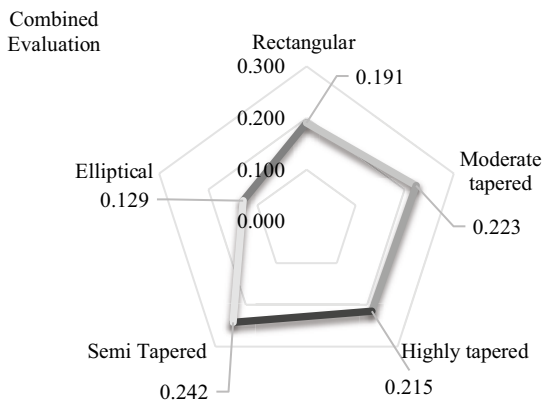


Figure 13. AHP result based on combined result

3.2. Thickness of an airfoil

Figures 14–19 show the effect of increasing thickness of an airfoil over the wing design using AHP technique. AHP results of change in thickness of airfoil are slightly similar with the effect of camber. The surface area increases with the thickness of an airfoil and it is directly associated with the lift. The parasitic drag is associated with the shape of moving body and skin friction of body with fluid. After

certain value of an airfoil thickness (above 21% of chord), the parasitic drag increases and it affects the lift generation. Moderate airfoil thickness (12–21% of chord) provides the better lift to drag efficiency and shows smooth stall characteristics. Increased thickness provides large internal volume which can be used for more fuel storage, but it requires more stiff design of wing structure, parallelly rise in the maximum take-off weight of an aircraft.

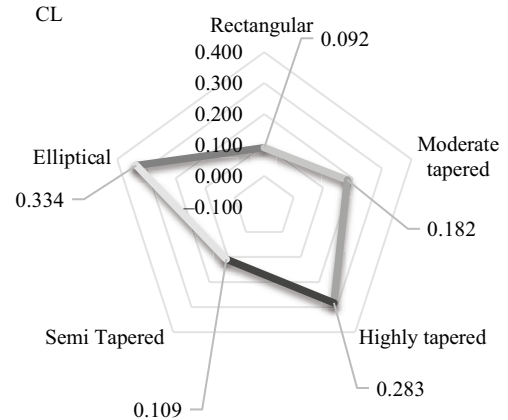


Figure 14. AHP result based on coefficient of lift

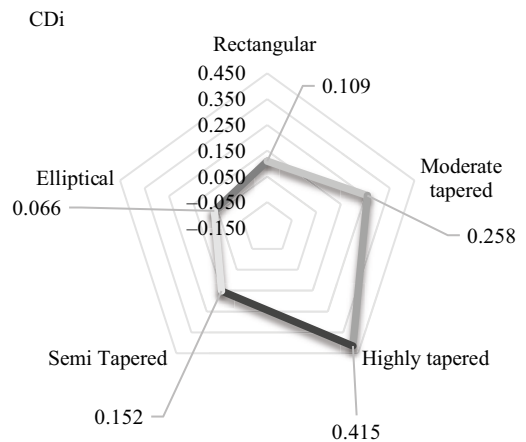


Figure 15. AHP result based on coefficient of induced drag

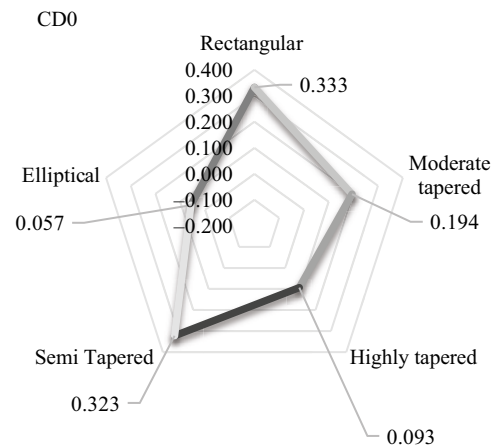


Figure 16. AHP result based on coefficient of parasitic drag

This type of the wings can be used for slower flights and for an aircraft which require less manoeuvrability. Use of these airfoils depend upon an application and operating conditions.

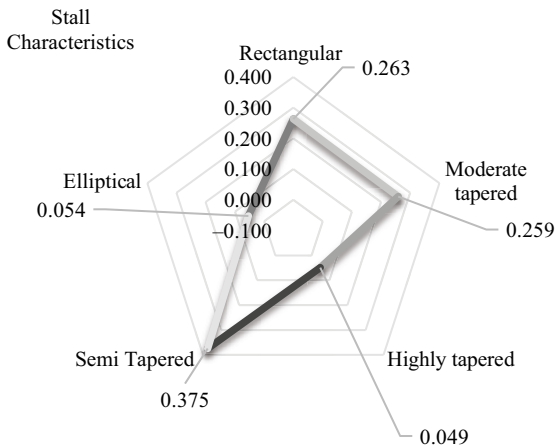


Figure 17. AHP result based on stall characteristics

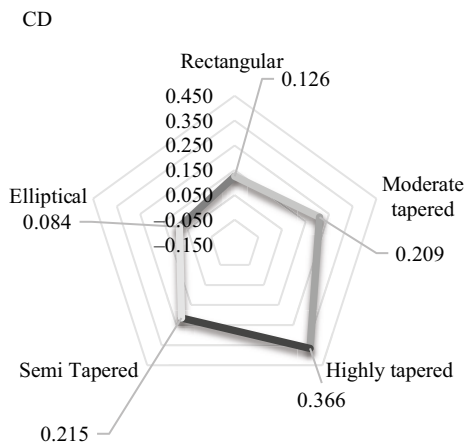


Figure 18. AHP result based on coefficient of total drag

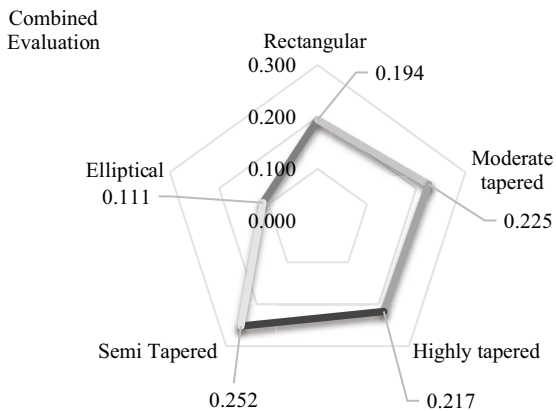


Figure 19. AHP result based on combined result

4. Conclusions

The innovative aspect of this study lies in the integration of computational analysis of wing planforms with AHP technique to investigate and compare various aerodynamic parameters of wing, which forms a systematic framework for decision making and determining an efficient wing design among the alternatives. The parameters as lift, drag and stall are determined using this technique which will help the UAV designer to choose the efficient wing planform and understand the behaviour of wing with different airfoils in the conceptual and preliminary design stage of an UAV. It has been observed that a semi tapered wing might be best possible design, when no sweep angle and dihedral angle involved. The lift of highly tapered and elliptical wings is high near the wing tip as these wings use the overall span effectively but are not good option because of the unstable stall characteristics. Rectangular wing planform provides good stall characteristic, but it is inefficient in producing lift as compared with highly tapered and elliptical wing. Moderate tapered ($\lambda = 0.5$) and semi tapered wing might be the better option to select the wing planforms, as these types of the wing planforms provide average lift coefficient in both the cases but are more efficient in stall characteristics which ensures the safer flight operations and are more controllable in stalling. The developed methodology helps in selection of most suitable wing design based on specific performance requirements, ensuring a balance between aerodynamic efficiency of a fixed wing UAV and flight safety.

Acknowledgements

This research received no external fundings. All the authors have no competing financial, professional, or personal interest from other parties.

References

- Akdeniz, H. (2020). A study on aerodynamic behavior of subsonic UAVs' wing sections with flaps. *International Journal of Aviation Science and Technology*, 2(1), 22–27. <https://doi.org/10.23890/IJAST.vm02is01.0103>
- Alam, G., Mamun, M., Ali, M., Islam, Q., & Islam, A. (2014). Investigation of the aerodynamic characteristics of an aerofoil shaped fuselage UAV model. *Procedia Engineering*, 90, 225–231. <https://doi.org/10.1016/j.proeng.2014.11.841>
- Bhushan, N., & Rai, K. (2004). *Strategic decision making applying the analytic hierarchy process*. Springer-Verlag. <https://doi.org/10.1007/b97668>
- Chen, T., & Katz, J. (2004). Induced drag of high-aspect ratio wings. In *42nd AIAA Aerospace Science Meetings and Exhibit*. ResearchGate. <https://doi.org/10.2514/6.2004-38>
- Daniel, S. J. (2020). Performance analysis of asymmetrical airfoil for subsonic flight using XFLR5 software. *International Journal of Progressive Research in Science and Engineering*, 1(8), 8–11.
- Das, S., & Roy, S. (2018). Finite element analysis of aircraft wing using carbon fiber reinforced polymer and glass fiber reinforced polymer. *IOP Conference Series: Materials Science and Engineering*, 402, Article 012077. <https://doi.org/10.1088/1757-899X/402/1/012077>

- Dhekane, T., & Sherje, N. (2020). CFD simulation of different taper ratio wings, performing trade-off assessment and development of a new methodology to plot lift distribution curve and 3D local coefficient of lift distribution graph. *International Journal of Engineering Research & Technology (IJERT)*, 9(04).
- Gudmundsson, S. (2022). Chapter 1 – The aircraft design process. In *General aviation aircraft design* (2nd ed., pp. 1–32). Elsevier. <https://doi.org/10.1016/B978-0-12-818465-3.00001-X>
- Guzelbey, I. H., Eraslan, Y., & Dogru, M. H. (2018). Effects of taper ratio on aircraft wing aerodynamic parameters: A comparative study. In *The 3rd International Mediterranean Science and Engineering Congress (IMSEC)*. ResearchGate. <https://doi.org/10.26701/ems.487516>
- Hamurcu, M., & Eren, T. (2020). Selection of unmanned aerial vehicles by using multicriteria decision-making for defence. *Journal of Mathematics*, 2020. <https://doi.org/10.1155/2020/4308756>
- Haque, M., Ali, M., & Ara, I. (2015). Experimental investigation on the performance of NACA 4412 aerofoil with curved leading edge planform. *Procedia Engineering*, 105, 232–240. <https://doi.org/10.1016/j.proeng.2015.05.099>
- Hospodář, P., Drábek, A., & Prachař, A. (2022). Aerodynamic design and strength analysis of the wing for the purpose of assessing the influence of the bell-shaped lift distribution. *Aerospace*, 9(1), Article 13. <https://doi.org/10.3390/aerospace9010013>
- Jadhav, B. (2020). Modeling and structural analysis of aircraft wing using aluminium alloy and titanium alloy. *International Research Journal of Engineering and Technology (IRJET)*, 7(12).
- Karpenko, M., Stosiak, M., Deptuła, A., Urbanowicz, K., Nugaras, J., Królczyk, G., & Żak, K. (2023). Performance evaluation of extruded polystyrene foam for aerospace engineering application using frequency analyses. *The International Journal of Advanced Manufacturing Technology*, 126, 5515–5526. <https://doi.org/10.1007/s00170-023-11503-0>
- Khan, M., & Faruk, A. (2018). Comparative analysis of aerodynamic characteristics of rectangular and curved leading edge wing planforms. *American Journal of Engineering Research (AJER)*, 7(5), 281–291.
- Kirubakaran, R., Dhakshinamurthy, L., Rajkumar, S., & Rajendran, A. (2017). Aircraft wing weight optimization by composite material structure design configuration. *IOSR Journal of Mechanical and Civil Engineering*, 14(6), 71–80.
- Lubecki, M., Stosiak, M., Skačkauskas, P., Karpenko, M., Deptuła, A., & Urbanowicz, K. (2022). Development of composite hydraulic actuators: A review. *Actuators*, 11(12), Article 365. <https://doi.org/10.3390/act11120365>
- Palcic, I., & Lalic, B. (2009). Analytical hierarchy process as a tool for selecting and evaluating projects. *International Journal of Simulation Modelling*, 8(1), 16–26. [https://doi.org/10.2507/IJSIMM08\(1\)2.112](https://doi.org/10.2507/IJSIMM08(1)2.112)
- Sadraey, M. (2013). *Aircraft design: A systems engineering approach*. John Wiley & Sons, Ltd. <https://doi.org/10.1002/9781118352700>
- Saraçyakupoğlu, T., Delibaş, H., & Özçelik, A. (2022). An experimental determination and numerical analysis of a loiter munition unmanned aerial vehicle system. *International Journal of 3D Printing Technologies and Digital Industry*, 6(1), 83–101. <https://doi.org/10.46519/ij3dptdi.1083686>
- Siddiqi, Z., & Lee, J. (2019). A computational fluid dynamics investigation of subsonic wing designs for unmanned aerial vehicle application. *Proceedings of the Institution of Mechanical Engineering Part G Journal of Aerospace Engineering*, 233(15). <https://doi.org/10.1177/0954410019852553>

Notations

Abbreviations

- AR – Aspect ratio;
 c – Chord;
 C₁ – Taper ratio correction factor;
 C_{Do} – Zero lift drag coefficient;
 C_l – Airfoil lift coefficient;
 C_L – Wing lift coefficient;
 C_{Lα} – Wing lift slope (/deg.);
 C_{lα} – Airfoil lift slope (/deg.);
 e – Oswald's span efficiency;
 K – Lift induced drag constant $\left(\frac{1}{\pi e AR}\right)$;
 t_{max} – Airfoil thickness;
 α – Angle of attack (deg.);
 α_{L=0} – Zero lift angle of attack (deg.);
 α_{Stall} – Stall angle of attack (deg.);
 α_{ZL} – Zero lift angle of attack for Mean geometric chord (deg.);
 Δα_{Stall} – Stall angle correction factor;
 λ – Taper ratio;
 Λ_{LE} – Leading edge sweep angle.